Heliyon 8 (2022) e09748

Contents lists available at ScienceDirect

Heliyon

journal homepage: www.cell.com/heliyon

Research article

Improvement of the mechanical properties and osteogenic activity of 3D-printed polylactic acid porous scaffolds by nano-hydroxyapatite and nano-magnesium oxide

Dian Xu [a,b], Zexian Xu [a,b], Lidi Cheng [a,b], Xiaohan Gao [a,b], Jian Sun [a,b,c,d,*], Liqiang Chen [a,b,c,d,**]

[a] The Affiliated Hospital of Qingdao University, Qingdao, 266003, China
[b] School of Stomatology, Qingdao University, Qingdao, 266003, China
[c] Dental Digital Medicine & 3D Printing Engineering Laboratory of Qingdao, Qingdao, 266003, China
[d] Shandong Provincial Key Laboratory of Digital Medicine and Computer-assisted Surgery, Qingdao, 266003, China

ARTICLE INFO

Keywords:
3D printing
nMgO
nHA
PLA
Tissue engineering scaffold
Osteogenesis
Crystallinity

ABSTRACT

Porous bone scaffolds based on high-precision 3D printing technology gave recently been developed for use in bone defect repair. However, conventional scaffold materials have poor mechanical properties and low osteogenic activity, limiting their clinical use. In this study, a porous composite tissue-engineered bone scaffold was prepared using polylactic acid, nano-hydroxyapatite, and nano-magnesium oxide as raw materials for high-precision 3D printing. The composite scaffold takes full advantage of the personalized manufacturing features of 3D printers and can be used to repair complex bone defects in clinical settings. The composite scaffold combines the advantages of nano-hydroxyapatite, which improves the formability of scaffold printing, and of nano-magnesium oxide, which regulates pH during degradation and provide a good environment for cell growth. Additionally, nano-magnesium oxide and nano-hydroxyapatite have a bidirectional effect on promoting the compressive strength and osteogenic activity of the scaffolds. The prepared composite porous scaffolds based on 3D printing technology show promise for bone defect repair.

1. Introduction

3D printing technology, as an emerging manufacturing technology, is being widely used in the biomedical field due to its high flexibility and personalization capacity in product manufacturing. Numerous studies have shown that porous scaffolds can be effectively used in bone defect repair (Bose et al., 2013). 3D printing technology, as an emerging manufacturing technology, is being widely used in the biomedical field due to its high flexibility and personalization capacity in product manufacturing. Numerous studies have shown that porous scaffolds can be effectively used in bone defect repair (Bose et al., 2013). 3D printing technology allows for precise design of scaffolds, overcoming many of the drawbacks of traditional fabrication methods. In the field of bioengineering, numerous biomaterials such as hydrogels, biodegradable materials, and metal materials have proven to be ideal raw materials for 3D printing. Nevertheless, there is a mismatch between the materials commonly used for direct 3D printing of bone repair scaffolds and the need to obtain nanostructured materials prepared with biomaterials for bone regeneration; therefore, the development of nanostructured biomaterial bone scaffolds is urgently necessary (Meng et al., 2012). Ideally, scaffold for bone tissue regeneration need to have mechanical properties that match the corresponding tissue to reduce the stress–strain imbalance. Furthermore, material degradability and the effect of degradation products are also of concern.

Poly-l-lactic acid (PLA) has been widely used in the field of tissue engineering due to its good biocompatibility and degradability (Zahedi, 2019). It is approved as an implant by the Food and Drug Administration (Naghieh et al., 2017; Tyler et al., 2016). Current biodegradable materials that can be used as implants are mainly divided into non-metallic degradable materials and metallic degradable materials, such as PLGA, PCL and magnesium-based materials. In contrast, PLGA is costly and difficult to synthesise; PCL is too fluid and difficult to shape when used for 3D printing; and magnesium-based metal materials produce a lot of hydrogen and degrade too quickly when implanted in the human body. Therefore, PLA is the more desirable raw material for tissue engineering scaffolds. Moreover, the excellent processing properties of PLA make it a

* Corresponding author.
** Corresponding author.
E-mail addresses: sunjianqdfy@qdu.edu.cn (J. Sun), clqiang1010@163.com (L. Chen).

https://doi.org/10.1016/j.heliyon.2022.e09748
Received 8 March 2022; Received in revised form 7 May 2022; Accepted 15 June 2022

potential raw material for 3D printing (On et al., 2020). However, the application of PLA directly as a 3D-printed scaffold for bone defect repair has various issues, in particular its poor mechanical properties. and its poor osteogenic activity, limiting its clinical application. Furthermore, lactic acid, a degradation product of PLA, accumulates in local tissues, lowering the pH of body fluids and affects cell growth as well as eventually leading to scaffold implantation failure (James et al., 2012; Zhao et al., 2018).

The addition of inorganic fillers to the raw materials for 3D printed PLA scaffolds improves its mechanical properties (Aworinde et al., 2020; Xia et al., 2019). Hydroxyapatite is the main component and crystal structure similar to biological hydroxyapatite of human hard tissues and has been regarded as an ideal material for bone repair for many years. Hydroxyapatite can be used as an additive to modify common 3D promised biological raw materials, increasing the mechanical properties and osteogenic activity of the material (Swain et al., 2021). Nano-HA (nHA) has better bioactivity and promotes bone regeneration to a greater extent than normal HA (P. Feng et al., 2020; Mohd Zaffarin, Ng, Ng, Hassan and Alias, 2021; Nonoyama et al., 2021). Incorporating nHA as an inorganic filler can significantly improve the mechanical strength of PLA scaffolds (Hassanajili et al., 2019). In addition, nano-magnesium oxide (nMgO), a common inorganic filler, has been shown to increase the mechanical properties of PLA scaffolds (Pei et al., 2010; Yun et al., 2016). As an alkaline oxide, MgO can neutralize the acidic products of PLA during degradation, resulting in a weakly alkaline local tissue process that promotes osteoblast growth. At the molecular level, magnesium ions are involved in various enzymatic reactions in cells and can indirectly encourage cell mineralization by increasing the activity of alkaline phosphates (C. Feng et al., 2017; Lin et al., 2018; Park et al., 2010; Serre et al., 1998; Tarafder et al., 2013). In addition, it has been shown that the incorporation of MgO into PLA can significantly increase the activity of osteoblasts and can effectively inhibit the value-added of osteoclasts, providing a good physiological basis for bone regeneration, in addition to the powerful antibacterial activity that MgO provides to PLA(Aničić et al., 2021). Other common dopants of PLA composites are ZnO and CuO, among others.

ZnO, as a dopant with the same potential as magnesium oxide, is slightly less chemically active than MgO, is an amphoteric oxide, and as a dopant cannot neutralize the acid produced by PLA degradation. Although Cu has good antibacterial effect, it is seldom used as composite scaffold dopant because Cu^{+} are heavy metal ions and long-term accumulation in human body is easy to lead to heavy metal poisoning.

The internal structure of 3D-printed composite scaffolds is critical for the mechanical properties and bioactivity of the scaffold. A high porosity promotes cell adhesion and value addition but at the same time reduces mechanical strength (Holmes et al., 2016). Therefore, in the design phase of 3D printing, the internal structure of the scaffold needs to be optimized while ensuring high porosity to meet the requirements for bone defect repair (C. Feng et al., 2017). Due to the high fluidity of PLA, the formability is often poor when printing high precision models (Frone et al., 2019). Therefore, ultra-high precision bio-3D printers are needed to ensure the quality of the finished products.

In this study, a new 3D-printed composite material consisting of a PLA matrix with nHA and nMgO fillers was designed. Through the assessment of the effect of combined nHA and nMgO as fillers, a new composite scaffold with high strength and personalization was thus constructed by digital model design and 3D printing technology. In addition, the degradation properties, mechanical properties, hydrophilicity, and osteogenic activity of the composite scaffolds were investigated. Thus, the application of high-precision 3D printing technology provides new scaffolds for tissue engineering repair of bone defects.

2. Materials and methods

2.1. Materials

PLA particles were provided by Nature Works (USA, M_w 50,000 Da, purity ≥98wt%). nHA (grain size <100 nm; purity ≥97wt%) was obtained from Shanghai Aladdin Biochemical Technology Co. Ltd. (Shanghai, China). nMgO (grain size, 20 nm; purity 98wt%) was purchased from Nanjing XFnano Ltd. (Nanjing, China). Mouse embryonic osteoblasts were obtained from Shanghai Bangjing Industry Co. Ltd. (Shanghai, China). Alkaline phosphatase (ALP) was detected using an ALP staining kit (DaLian Meilunbio Technology Co. Ltd.; Dalian, China). All materials were used directly without secondary processing.

2.2. Preparation of 3D printing nano-composite consumables

According to previous studies, HA at a mass fraction of 20% can significantly improve the mechanical properties of PLA (Russias et al., 2006). MgO at 3% mass fraction can significantly promote the crystalline and mechanical properties of PLA (Shuai et al., 2019b). According to the stated composition in Table 1, granular PLA, nHA powder, and nMgO powder were added to 98% anhydrous ethanol and stirred magnetically at 60 °C for 2 h, and ultrasonically dispersed for 1 h. The resulting mixed solution was placed in a drying oven for 12 h to obtain a solid mixed material. Finally, the mixture was ground in a mill for 2 h to obtain 3D printing composite consumables.

2.3. Design and printing of nano-composite scaffolds

The supports used in this study were designed using 3D Studio Max (3D Max) software. The composite material was printed into a 3D porous structure using the fused deposition method, with a print line width of 0.25 mm, a line spacing of 0.5 mm, and a cross-grid structure for inside support. The created bracket model was exported in rapid prototype format (.stl file) and imported into the fused deposition printer (Qingdao 5D Intelligent Additive Manufacturing Technology Co., Ltd., China) with the printing temperature controlled at ~180 °C. The whole process is shown in Figure 1.

2.4. Characterization of the nano-composite scaffold

The phase structure of the scaffolds was characterized using an X-ray diffractometer (X'Pert PRO MPD Panalytical B.V) at a scanning rate of 8°/min from 10° to 80°. The nano-composite scaffolds were analyzed by Fourier transform-infrared (FTIR) spectroscopy (Nicolet iS 10 Thermo Fisher Scientific, USA) within the range of 500–4000 cm^{-1}. The surface of the nano-composite scaffold was observed with high-resolution scanning electron microscopy (SEM; Hitachi S4800). The water contact angle on the surface of the stent was tested with an optical tensiometer (Biolin Scientific Co. Ltd., Sweden) to analyze the hydrophilicity of the stent.

2.5. Compression test of the nano-composite scaffold

The scaffold compression test was conducted on a universal testing machine (MTS Systems, Co., Ltd. China) with a compression rate of 0.5 mm/min and a compression amount of 50%. The compressive stress at the time of bracket fracture was recorded and the stress–strain curve was plotted to derive the compressive modulus of the bracket. All samples were tested in a dry environment at room temperature, six times.

2.6. Thermal property analysis

Thermogravimetric analysis was performed using the TG NETZCSCH DSC214 (Germany) system. The crystallization properties of the prepared PLA, PLA/nHA, and PLA/nHA/nMgO scaffolds were studied by a non-isothermal crystallization process using differential scanning calorimetry (DSC). The activated scaffolds were ramped up to 200 °C at a rate of 10 °C/min in an argon atmosphere, held for 5 min, and then reduced to 40 °C at a rate of 10 °C/min. The DSC curves of the samples were subsequently recorded. The thermal stability and crystallization behavior of the tested samples were analyzed by DSC.

Table 1. Formulation composition of 3D printing composite consumables.

Samples	PLA(wt%)	nHA(wt%)	nMgO(wt%)
PLA	100	0	0
PLA/nHA	80	20	0
PLA/nHA/nMgO	77.6	19.4	3

2.7. Degradation test and immersion acidity test

The composite scaffolds were dried and weighed and their mass recorded as W_0, after which they were completely immersed in PBS (37 °C, pH 7.4) solution, changed twice a week; after 7, 14, 21 and 28 days of immersion, the scaffolds were removed, dried, and weighed and recorded as W_t. The weight loss rate was calculated and recorded as W_L according to the following Eq. (1):

$$W_L = \frac{(W0 - Wt)}{W0} \times 100\% \quad (1)$$

pH assays were performed in simulated body fluids, and the scaffolds were immersed in simulated body fluids for 7, 14, 21 and 28 days. The pH of the solution was detected and recorded.

2.8. Cytotoxicity assay

Mouse embryonic osteoblast precursor cells (MC3T3-e1) were used as experimental cells. Dulbecco's modified Eagle's medium (DMEM) supplemented with 10% (*v/v*) fetal bovine serum and 1% (*v/v*) penicillin-streptomycin solution was used as the medium for experimental cells. All composite scaffolds are subjected to a rigorous autoclave process before seeding. The scaffolds was cut into squares with 5 mm sides and placed in a 64-well plate. MC3T3-E1 cells were inoculated in 64-well plates at ~5000 cells per well and co-cultured with the scaffolds for 1, 3, and 5 days. The scaffolds were then removed, and the cells were rinsed twice with PBS solution. Observed by cell staining with an inverted fluorescent microscopeand. Following co-culture of the scaffolds with MC3T3-E1 cells for 1, 3, and 5 days, the cells were rinsed twice with PBS solution, incubated for 2 h with 2 mL of CCK-8 reagent in the medium to assess cell viability, and an enzyme marker measured the absorbance value at 450 nm.

2.9. Osteogenic activity

The early osteogenic activity of the nano-composite scaffold was evaluated by measuring the ALP content. MC3T3-E1 cells were co-cultured with the nano-composite scaffolds in osteogenic induction medium (10% PBS, 10 mmol/L β-glycerophosphate sodium, 10 mmol/L dexamethasone, and 0.05 mmol/L ascorbic acid) for 7 and 14 days, and the scaffolds were then removed and rinsed twice with PBS solution. Cells were fixed with 4% paraformaldehyde solution and stained with an ALP stain at 37 °C. ALP activity in the stained samples was observed by inverted fluorescence microscopy, followed by quantitative analysis of ALP activity.

The late osteogenic activity of the nano-composite scaffold was assessed by measuring the content of calcareous nodules. The medium used was of the same composition as that used for ALP activity, and the scaffolds and cells were co-cultured for 21 days and then rinsed twice with the same PBS solution. Cells were fixed with 4% paraformaldehyde, stained with alizarin red dye at room temperature, and the number of calcium nodules in the stained samples was observed with an inverted fluorescence microscope. After staining with Alizarin Red, the cells were washed with buffer and the amount of intracellular calcium deposited was measured at 420nm using an enzyme-linked immunosorbent assay.

2.10. Statistical analysis

All quantitative data were expressed as mean ± standard deviation. All data were analyzed by one-way analysis of variance (ANOVA) using SPSS22. A p value of <0.05 was considered statistically significant.

3. Result and discussion

3.1. Characterization of the nano-composite scaffold

The prepared 3D porous composite scaffold had an average pore size of 0.5 mm (Figure 2A), which can greatly promote cell adhesion and growth. providing a stable space for osteoblast growth. SEM images of the three sets of scaffolds at different magnifications were obtained (Figure 2B). The composite scaffolds with nHA and nMgO showed better plasticity than that composed of pure PLA. nMgO on the scaffold surface can be seen under high magnification.

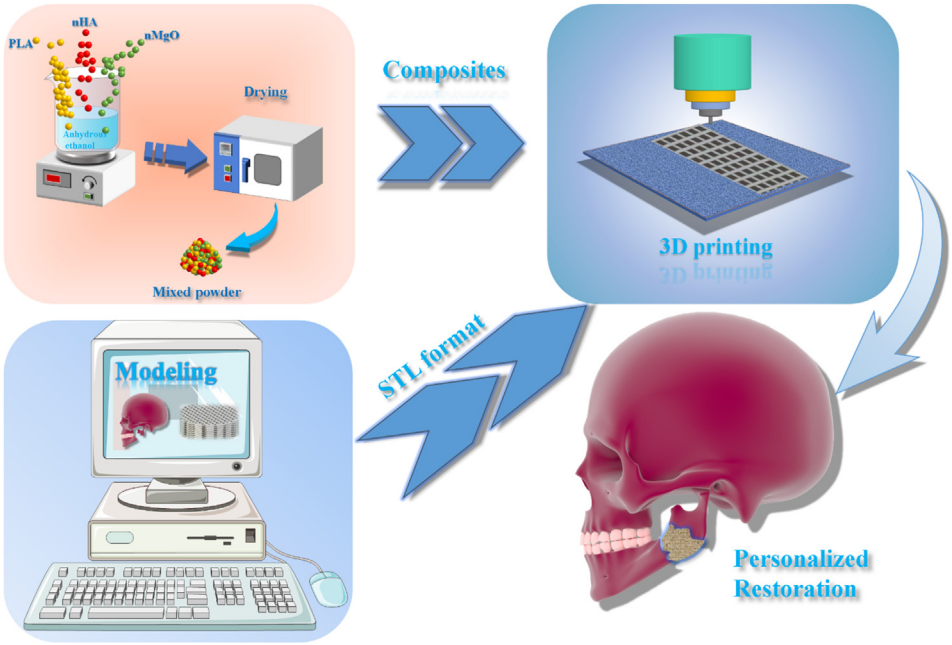

Figure 1. Schematic diagram of a personalized tissue-engineered bone composite scaffold using 3D printing technology.

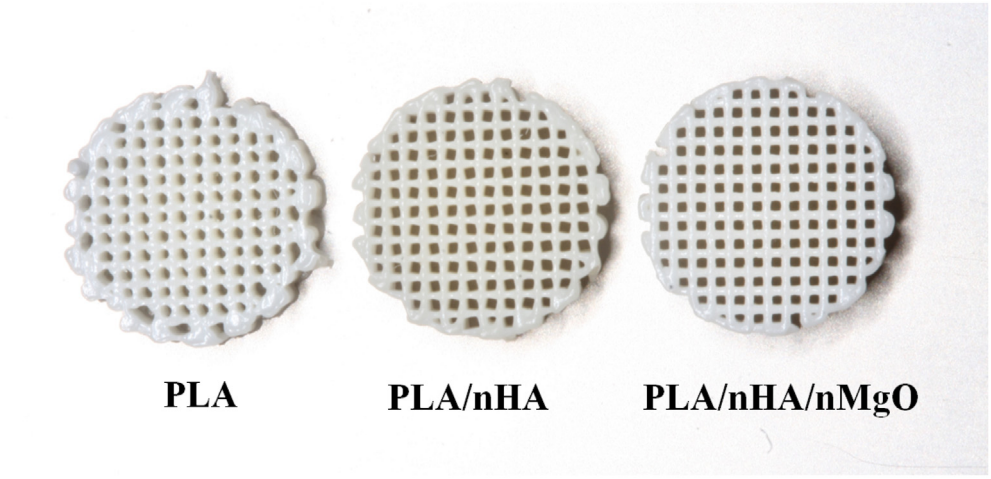

(A)

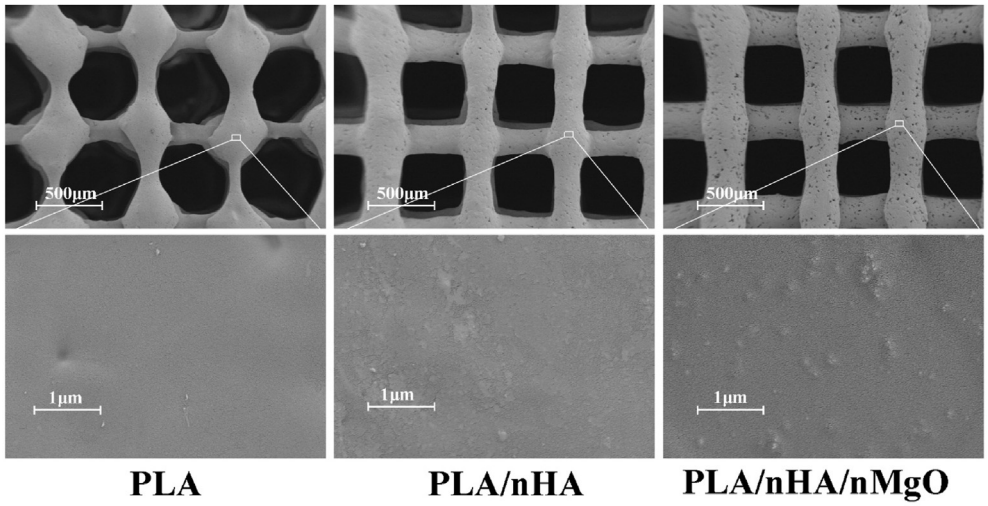

(B)

Figure 2. Composite bracket actual photo (A); Scanning electron microscopy (SEM) observed the surface morphology of three groups of seed scaffolds (B).

The FTIR spectra for each scaffolds and raw materials were obtained (Figure 3A). The hydroxyl band of the HA powder was observed at 606 cm^{-1}. The pure PLA scaffold showed a band at 1747 cm^{-1} corresponding to the carbonyl group, bands at 1390 cm^{-1} and 1430 $cm^{-1}$for $CH–CH_3$, at 1330 cm^{-1} for CH–C–O–O, and at 1160 cm^{-1} corresponding to C–O–C (Diez-Escudero et al., 2021). The corresponding hydroxyl reinforcement bands after the addition of HA are shown in the figure, and the corresponding reinforcement bands appear in the composite after the addition of nMgO.

XRD patterns of the composite scaffolds and raw materials were obtained (Figure 3B). Typical peaks were detected for all scaffolds. The characteristic peaks corresponding to MgO were detected at 42.9° and 62.2° following the addition of nMgO (Figure 3B). The composite scaffold showed a characteristic peak of HA at 31.8°. Thus, nHA and nMgO were successfully incorporated into PLA.

The water contact angle of the pure PLA scaffold was high, at more than 90° (Figure 3C), likely due to PLA lacking hydrophilic groups in its structure, resulting in a strong hydrophobicity on the material's surface (Shuai et al., 2019a). The water contact angle of the composite scaffold with the addition of nHA was significantly reduced, mainly attributed to the polar nature of HA with strong hydrophilic characteristics and the large number of active functional hydroxyl groups on its surface (Lu et al., 2020). Due to the enhanced intermolecular forces, such as van der Waals, nHA often agglomerates and forms micron-sized particles (Zhou et al., 2019). When HA and PLA are compounded, hydrophobic forces reduce their interaction, increasing their dispersion and exposing more hydroxyl groups on the surface. The water contact angle of the composite scaffold following the addition of nMgO was further reduced since the doping of nMgO changed the surface structure of the composite scaffold, allowing hydrogen bonding and increasing the hydrophilicity of the composite scaffold (Guan et al., 2001). Hydrophilic scaffolds are thought to facilitate cell adhesion and growth, thus promoting the regeneration of bone tissue (Guan et al., 2001; Li et al., 2020). In the study by Cijun Shuai et al. (2019b), the hydrophilic angle of the scaffold increased with the increase of MgO content when MgO was added directly among the scaffolds in pure PLA, which is basically consistent with the results obtained in the present study, and the difference in hydrophilic angle may be due to the different humidity of external air.

3.2. *Nano-composite scaffold compressive resistance*

Because the tissue-engineered scaffolds implanted in the human body need specific mechanical properties, compression tests were performed on each group of composite scaffolds to obtain stress–strain curves (Figure 4A). After analysis and calculation, the scaffold's yield strength were obtained (Figure 4B). The mechanical properties of the composite

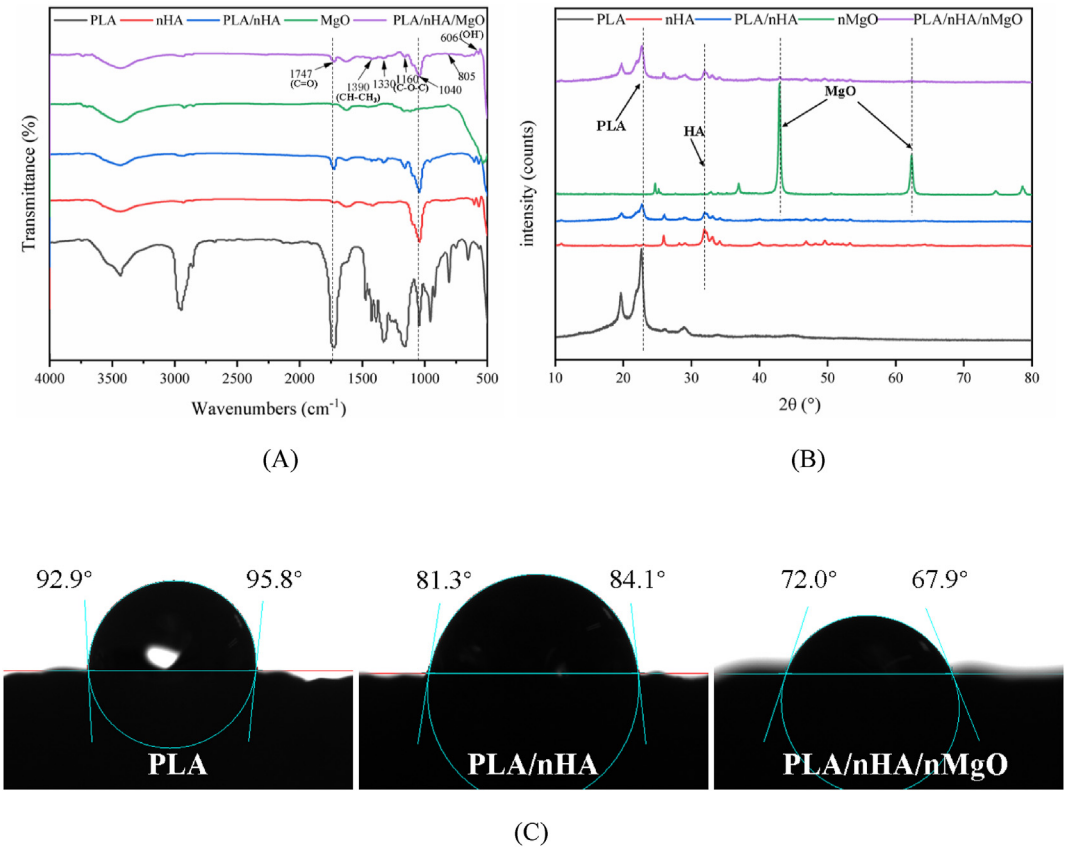

Figure 3. Fourier transform infrared spectrometer FTIR spectra of composite supports and raw materials (A); X-ray diffraction (XRD) spectra of composite supports and raw materials (B). Water contact angle of three groups of scaffolds (C).

scaffold were higher overall than those of the pure PLA scaffold. The yield stress of the pure PLA scaffold was of ~18 MPa, and the addition of nHA increased the yield gravitational force of the composite scaffold to 22 MPa, an overall improvement of ~22%. Of note, the yield stress of the composite scaffold increases to 24 MPa following the addition of nMgO, likely due to the nanoparticles dispersing in the material preventing the extension of cracks under external forces (Butt et al., 2017; Fletcher, 1958). We compared the mechanical properties of PLGA/HA/MgO made by simple casting methods. The compressive strength of the PLA scaffold incorporating hydroxyapatite and MgO in this study exceeded 20 MPa, a figure that exceeds the 16 MPa obtained in the literature (Hickey et al., 2015). HA is the main component of human cancellous bone, and the modified composite scaffold is well-matched to the high modulus of natural bone tissue, providing a stable environment for bone tissue regeneration.

3.3. Thermal behavior

The non-isothermal crystallization behavior of the composite scaffolds was investigated by DSC (Figure 5A). The thermal property parameters are shown in Table 2. The non-isothermal crystallization peaks of the three scaffolds appeared at shorter times, with half-crystallization times of 14.50 min, 14.36 min, and 14.22 min, respectively, indicating that the addition of nHA and nMgO slightly accelerated the

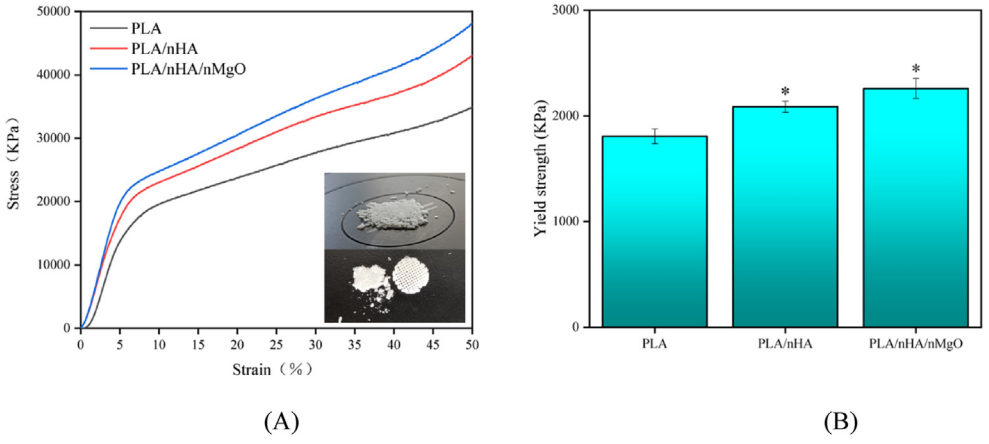

Figure 4. Compressive stress-strain curve of each group of scaffolds (A); Yield strength of each group of scaffolds (B).

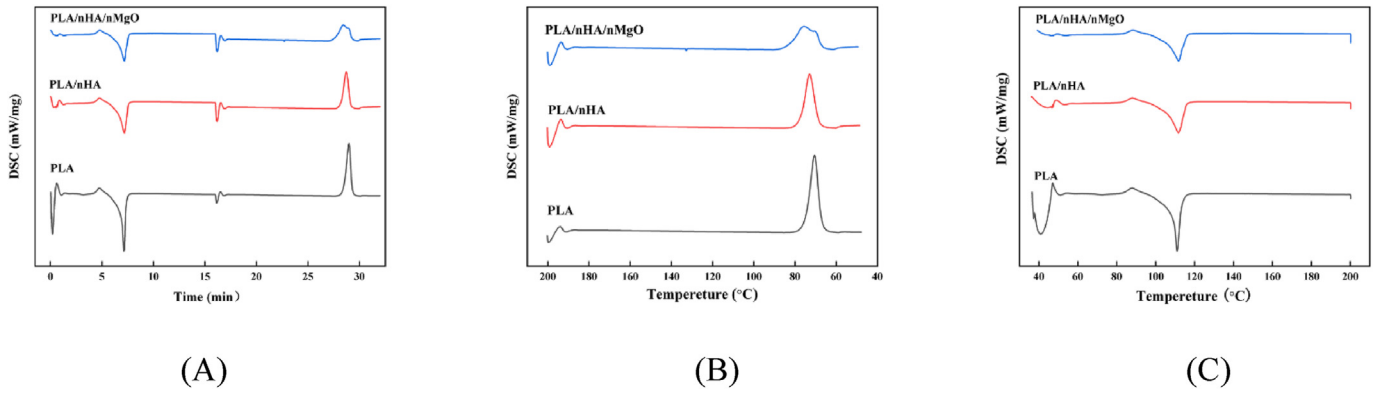

Figure 5. Differential scanning calorimetry (DSC) non-isothermal crystallization curve (A); Crystallinity curve (B); Melting Curve (C).

Table 2. The thermal performance parameters of PLA, PLA/nHA and PLA/nHA/nMgO were determined by differential scanning calorimetry.

Sample	Tm (°C)	Tc (°C)	ΔHm (J/g)	ΔHc (J/g)	Xc (%)	$t_{1/2}$ (min)
PLA	111.1	70.5	8.55	71.31	56.70	14.50
PLA/nHA	111.7	72.9	8.92	56.23	70.35	14.36
PLA/nHA/nMgO	111.8	75.6	6.69	45.6	50.40	14.22

crystallization rate of PLA. The warming melting curve and cooling crystallization curve of the composite scaffolds (Figures 5B and 5C, respectively) along with the data in Table 2, showed that the melting temperature (T_m) of the three samples did not vary much and was of ~111 °C. The melting enthalpy ΔH_m of the melting peaks was 8.55 J/g, 8.92 J/g, and 6.69 J/g (Figure 5C). Previous studies have shown that an increased crystallization temperature indicates a faster crystallization rate (Cebe and Hong, 1986; Masuko, 1998). The crystallization temperatures of the three groups of scaffolds were 70.5 °C, 72.9 °C, and 75.6 °C. rystallization peaks ΔHc were 71.31 J/g, 56.23 J/g, and 45.6 J/g, respectively, indicating that the addition of nHA and nMgO led to the easier crystallization of PLA. The $t_{1/2}$ (semi-crystallization time) and exothermic enthalpy (ΔHc) show some positive correlation. This indicates that the scaffold can reach the upper limit of crystallization faster from melting to molding during 3D printing of the raw material, and the high crystallinity promotes the mechanical properties of the composite. Combined with the degradation experiments, it can be concluded that HA and MgO can retard the degradation of PLA and maintain the early stability of the scaffold after implantation into the human body. The crystallization of polymers occurs through the ordered rearrangement of molecular chains; the addition of nanoparticles provides more nucleation sites for the original polymers and accelerates their crystallization rate. Overall, nMgO and nHA play a bi-directional role in promoting the scaffolds' thermal stability and crystallization properties.

3.4. Degradation behavior and PH-regulating properties

The degradation behavior of the composite scaffold was examined by a PBS solution immersion test (Figure 6A). All scaffolds showed degradation behavior over time, as evidenced by the reduction in scaffold weight. The lower weight loss of scaffolds with added nHA compared to pure PLA scaffolds was attributed to the dispersion of HA in PLA, reducing the direct contact area between PLA and PBS solution (Houaoui et al., 2020). Notably, the degradation rate of the scaffold compounded with nMgO was significantly retarded. The addition of HA effectively slows down the in vitro scaffold degradation rate and ensures the early stability following implantation in humans (Wang et al., 2010). The incorporation of nMgO also slowed down the degradation of the scaffold, likely due to a reduction in the amorphous region of the composite during the crystallization process and an improvement of stability of the composite scaffold. After 3 weeks of immersion, the degradation rate of the composite scaffold incorporating nMgO was significantly accelerated, likely due to the accelerated onset of degradation by OH^- generated by the hydration of MgO (Shuai et al., 2018; Zhao et al., 2017).

The pH changes of the scaffolds immersed in simulated body fluid were assessed (Figure 6B). The H^+ produced during the degradation of PLA lowers the pH of the body fluid; too low a pH can inhibit a variety of enzymatic reactions in the body, thus affecting osteoblast regeneration.

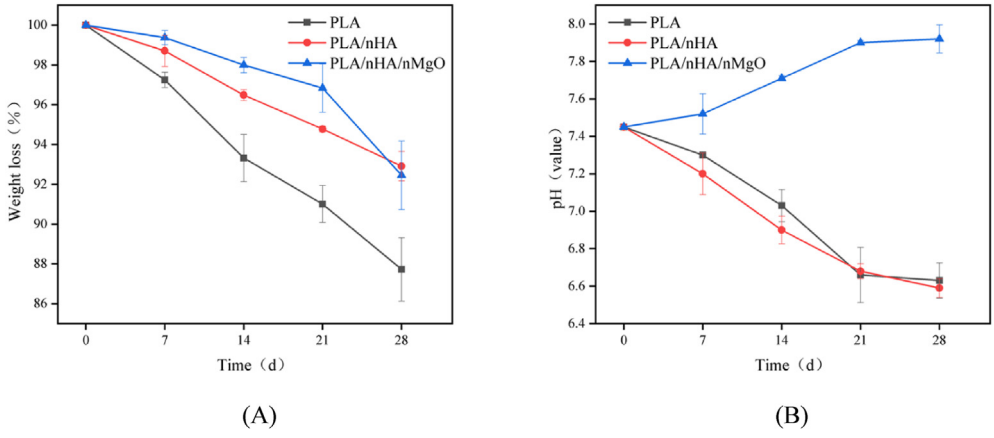

Figure 6. Weight loss (A) and PH change (B) of each group of scaffold immersion.

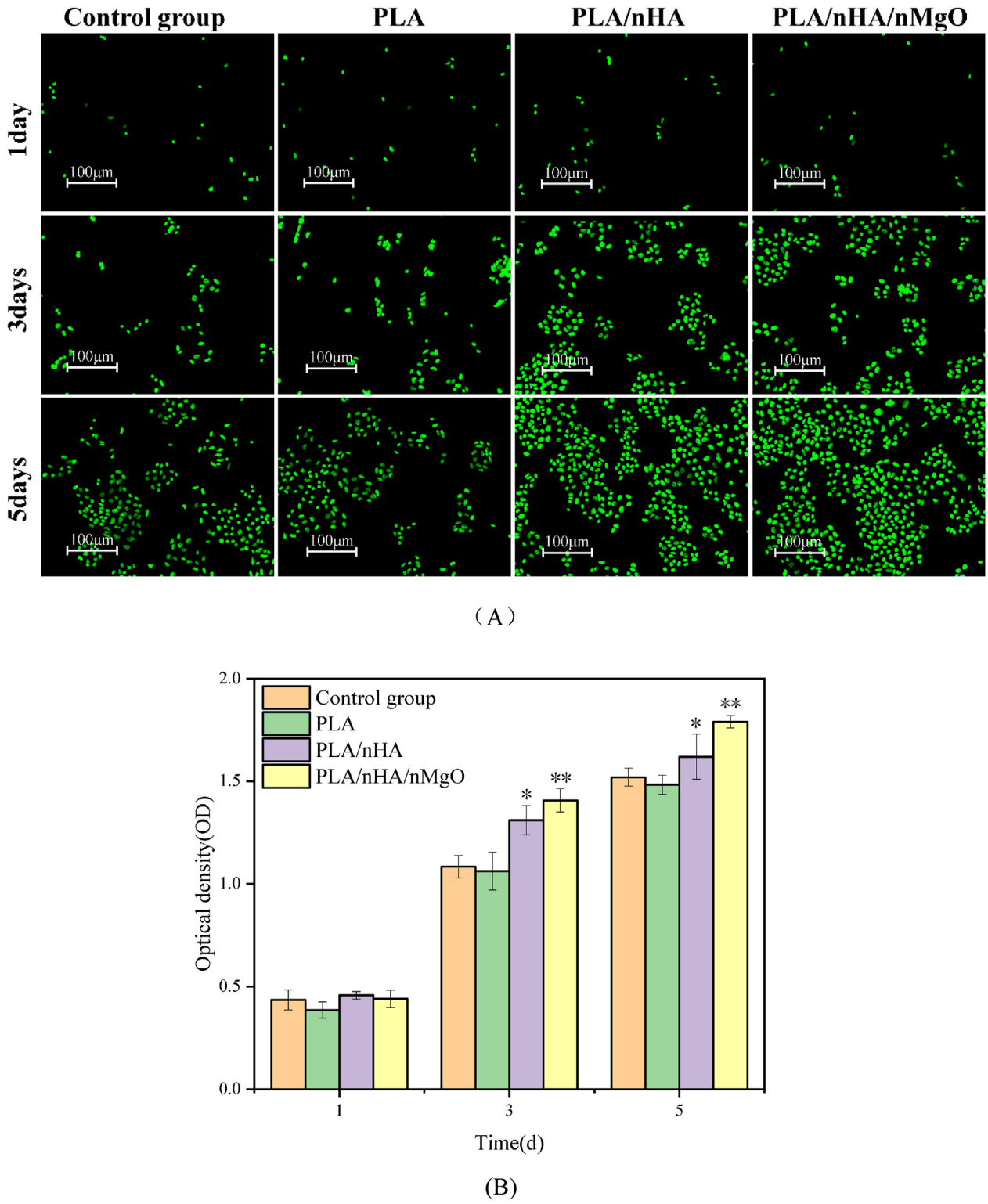

Figure 7. Fluorescence images (A) of MC3T3-E1 cells and optical density obtained by CCK-8 analysis (B).

The weak alkalinity created by the hydration of MgO can effectively neutralize the acidic products of PLA. The pH of the nMgO composite scaffold was maintained at ~7.4 after 28 days, and this data of pH was significantly higher compared with the PLA scaffold alone, and the difference was statistically significant ($p < 0.05$). The weak alkalinity can provide a stable pH environment for the regeneration of osteoblasts and promote bone healing (Gong et al., 2021; Tan et al., 2018; Yuan et al., 2018). In the research by Lizhe He et al. (He et al., 2021), the pH of polylactic acid composite scaffolds doped with magnesium oxide had increasing pH throughout the degradation process, a trend consistent with the results of the present study.

3.5. Cellular vitality

The viability of cells cultured on the composite scaffolds was tested by the CCK8 assay (Figure 7B). Following co-culture of MC3TC-E1 cells with

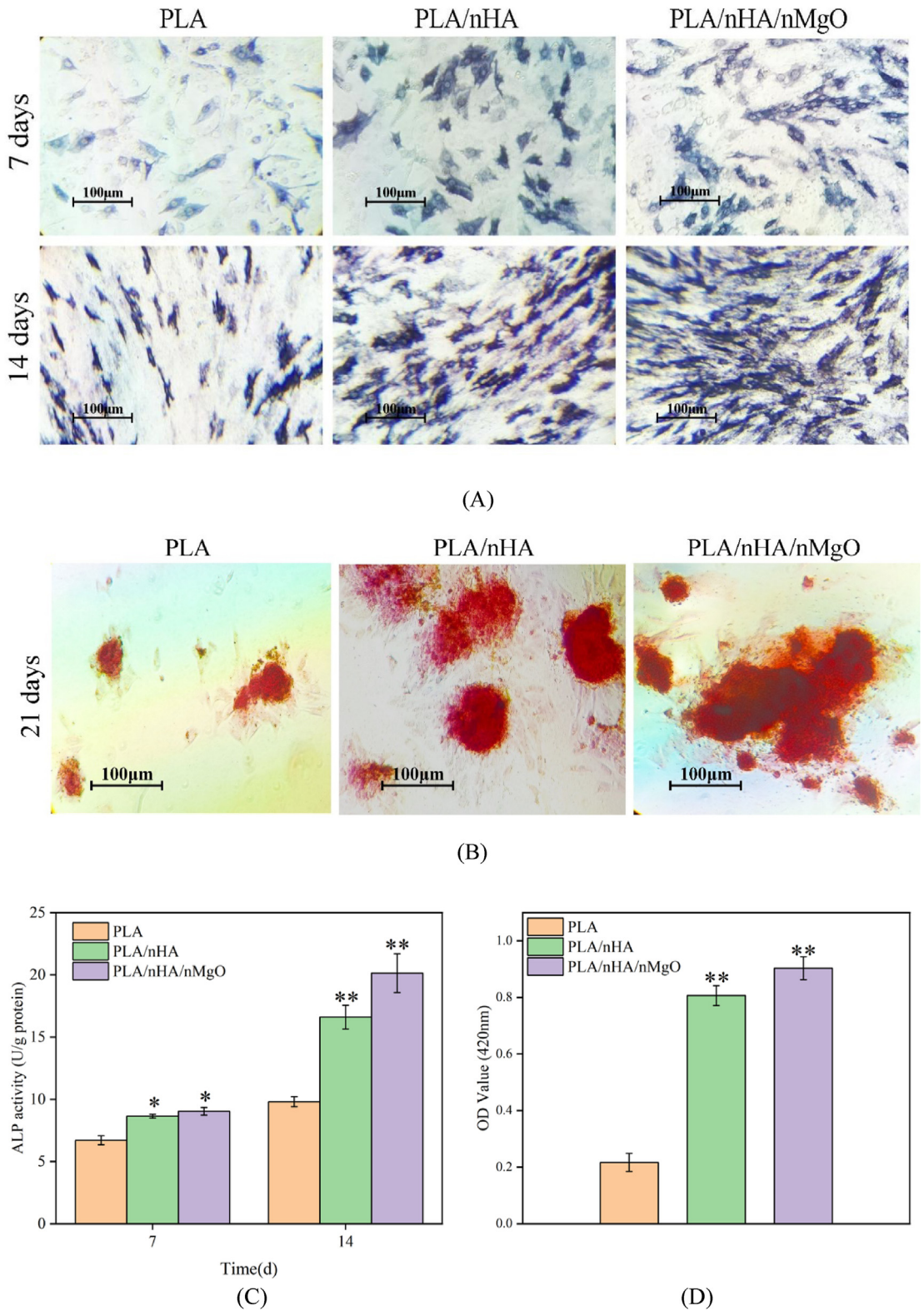

Figure 8. The ALP staining (A) and activity (C) after MC3T3-E1 cells cultured for 7 and 14 days; Alizarin red staining (B) and OD values (D) after 21 days of incubation (B).

the scaffold for 1 day, there was no significant difference in optical density (OD) values between the groups, likely due to the fact that the early stages of cell growth are less affected by the external environment. It is noteworthy that, from day 3 onwards, the OD values showed significant differences. The low OD of the PLA scaffold alone compared to the blank control group ($p < 0.05$) may be due to the inhibition of cell growth by the acidic products following PLA degradation. Scaffolds containing nHA exhibited greater cell viability, associated with calcium ions produced in water dispersed by nHA. It is well known that calcium ions are indispensable for cell growth, and they maintain the potential difference between the two sides of the cell membrane. Relevant studies have shown that calcium ions can activate enzymes related to signal

transduction and participate in several physiological processes such as cell metabolism and growth (Atif et al., 2021). The addition of nMgO further increased the OD value of the cells, mainly due to the hydrolysis of nMgO into $Mg(OH)^{-}$, which neutralizes the acidic by-products of PLA degradation and improves the environment for cell growth. In addition, magnesium ion promote the value-added of cells by increasing intracellular epidermal growth factor (EGF) and mitogens (Grubbs, 1991; Raisz, 1969; Zreiqat et al., 2002). Overall, both nHA and nMgO have good biocompatibility, reducing the cytotoxicity of PLA, regulating cell behavior, and promoting cell growth.

Fluorescence staining images of M3CT3-E1 cells showed that cells grown in all scaffolds had good biocompatibility (Figure 7A). After 1 day of co-culture, a small number of viable cells could be seen in all scaffolds, and the number of viable cells gradually increased as time progressed. After 3 and 5 days of culture, the number of cells on the nHA scaffold was significantly higher than that of the PLA scaffold. The composite scaffold with nMgO had significantly more live cells than the other two groups, indicating that the co-addition of nMgO and nHA had the most significant growth-promoting effect on cells. These results were generally consistent with those previously obtained with the CCK-8 assay. Thus, nMgO and nHA can jointly increase the activity of osteoblasts, which is consistent with the results of this experiment (Cui et al., 2020; Liu et al., 2020).

3.6. Osteogenic activity

According to previous studies, Mg, as an essential element for the human body, plays a significant role in osteogenesis According to previous studies, Mg, as an essential element for the human body, plays a significant role in osteogenesis (Wagener et al., 2016). In the present study, the osteogenic activity of the composite scaffold was evaluated by measuring the ALP content. Following co-culture of the composite scaffold with MC3T3-E1 cells for 7 days, the staining intensity of the nHA scaffold was significantly greater than that of the pure PLA scaffold, while the addition of nMgO had a minimal effect on the staining intensity (Figure 8A). After 14 days of co-culture of scaffolds and cells, the staining intensity was significantly increased for the nMgO scaffold, indicating that nMgO mainly acted at the late osteogenic stage, and the quantitative ALP analysis was consistent with the staining results. Thus, these results confirm the promoting role of nHA and nMgO in osteogenesis, and it has been shown that HA, as the main inorganic component of human bone, not only provides support for bone in terms of mechanical properties but also releases trace ions to induce bone regeneration.

The late-stage osteogenic activity was determined by detecting the deposition of calcium nodules after 21 days of cell culture. Red deposits of calcium nodules were visible for all scaffolds, with relatively few calcium nodules in the pure PLA scaffolds, followed by the PLA/nHA scaffold, and finally the PLA/nHA/nMgO scaffold (Figure 8B). The calcium nodules content intuitively shows the superiority of composite scaffolds in osteogenic differentiation, suggesting that both nMgO and nHA can promote the differentiation of osteoblasts and show a bidirectional promotion effect. The results confirmed the osteogenic ability of nMgO and nHA by measuring the absorbance values of alizarin red at 420 nm.

In recent studies, magnesium oxide nanoparticles have been used in various composites, and Salamanca, E et al. (Salamanca et al., 2022), used magnesium oxide to modify β-tricalcium phosphate to enhance osteoblast activity. Chen, Y et al. (Chen et al., 2022), doped magnesium oxide nanoparticles into composite hydrogels and promoted osteogenic differentiation of MC3T3-E1 cells by modulating the release of magnesium ions and upregulating the expression of osteogenic genes such as BSP and OPN. These studies are consistent with the present findings and confirm the great role played by magnesium in the osteogenesis process.

4. Conclusion

This study prepared a 3D porous composite scaffold containing PLA matrix, nHA, and nMgO using a high-precision 3D melt-forming printer. The composite scaffold had a porous structure that promotes the adhesion and growth of adult cells, a concept that has been confirmed in cytotoxicity experiments. In addition, the crystallinity and mechanical properties of the composite scaffold were greatly improved, and the composite scaffold prepared by 3D printing ensured the early stability after implantation into the human body compared with other different preparation methods. In pH adjustment experiments, we found that the pH of the composite scaffold doped with magnesium oxide was around 7.7–7.8 at around 21 days. The increase in pH was favourable to the growth of osteoblasts and the osteoblasts could mineralise effectively at pH = 8.0 (Galow et al., 2017). Of note, nMgO do not seem to play a role in the early Stage of osteogenic differentiation, likely due to the slow decomposition rate of the material and the small degree of hydrolysis of the nanoparticles, a speculation that cannot yet be fully confirmed from the current experimental data and requires further q-PCR and Western Blot experiments. In conclusion, nMgO and nHA have a bidirectional promotion effect on osteoblast differentiation. The 3D-printed PLA, nHA, and nMgO composite scaffolds have good mechanical properties, hydrophilicity and osteogenic activity, and have great potential in the field of bone defect repair.

Declarations

Author contribution statement

Dian Xu: Performed the experiments; Wrote the paper.

Zexian Xu: Analyzed and interpreted the data.

Lidi Cheng, Xiaohan Gao: Contributed reagents, materials, analysis tools or data.

Jian Sun, Liqiang Chen: Conceived and designed the experiments.

Funding statement

This work was supported by Qingdao Medical and Health Research Program Project (2021-WJZD193), and by Clinical Medicine + X Programme at Qingdao University Hospital for funding (QDFY+X2021 01041).

Data availability statement

Data will be made available on request.

Declaration of interests statement

The authors declare no conflict of interest.

Additional information

No additional information is available for this paper.

References

Aničić, N., Kurtjak, M., Jeverica, S., Suvorov, D., Vukomanović, M., 2021. Antimicrobial polymeric composites with embedded nanotextured magnesium oxide. Polymers 13 (13).

Atif, A., Pujari-Palmer, M., Tenje, M., Mestres, G., 2021. A microfluidics-based method for culturing osteoblasts on biomimetic hydroxyapatite. Acta Biomater. 127, 327–337.

Aworinde, A., Adeosun, S., Oyawale, F., Emagbetere, E., Ishola, F., Olatunji, O., Akinlabi, E., 2020. Comprehensive data on the mechanical properties and biodegradation profile of polylactide composites developed for hard tissue repairs. Data Brief 32, 106107.

Bose, S., Vahabzadeh, S., Bandyopadhyay, A., 2013. Bone tissue engineering using 3D printing. Mater. Today 16 (12), 496–504.

Butt, M.S., Bai, J., Wan, X., Chu, C., Xue, F., Ding, H., Zhou, G., 2017. Mechanical and degradation properties of biodegradable Mg strengthened poly-lactic acid composite through plastic injection molding. Mater. Sci. Eng. C 70, 141–147.

Cebe, P., Hong, S.D., 1986. Crystallization behaviour of poly(ether-ether-ketone). Polymer 27 (8), 1183–1192.

Chen, Y., Sheng, W., Lin, J., Fang, C., Deng, J., Zhang, P., Zeng, H., 2022. Magnesium oxide nanoparticle coordinated phosphate-functionalized chitosan injectable

hydrogel for osteogenesis and angiogenesis in bone regeneration. ACS Appl. Mater. Interfaces 14 (6), 7592–7608.
Cui, L., Zhang, J., Zou, J., Yang, X., Guo, H., Tian, H., Chen, X., 2020. Electroactive composite scaffold with locally expressed osteoinductive factor for synergistic bone repair upon electrical stimulation. Biomaterials 230, 119617.
Diez-Escudero, A., Andersson, B., Persson, C., Hailer, N., 2021. Hexagonal pore geometry and the presence of hydroxyapatite enhance deposition of mineralized bone matrix on additively manufactured polylactic acid scaffolds. Mater. Sci. Eng. C Mater. Biol. Appl. 125, 112091.
Feng, C., Zhang, W., Deng, C., Li, G., Chang, J., Zhang, Z., Wu, C., 2017. 3D printing of Lotus root-like biomimetic materials for cell delivery and tissue regeneration. Adv. Sci. 4 (12), 1700401.
Feng, P., Peng, S., Shuai, C., Gao, C., Yang, W., Bin, S., Min, A., 2020. In situ generation of hydroxyapatite on biopolymer particles for fabrication of bone scaffolds owning bioactivity. ACS Appl. Mater. Interfaces 12 (41), 46743–46755.
Fletcher, N.H., 1958. Size effect in heterogeneous nucleation. J. Chem. Phys. 29 (3), 572–576.
Frone, A., Batalu, D., Chiulan, I., Oprea, M., Gabor, A., Nicolae, C., Panaitescu, D., 2019. Morpho-structural, thermal and mechanical properties of PLA/PHB/cellulose biodegradable nanocomposites obtained by compression molding, extrusion, and 3D printing. Nanomaterials 10 (1).
Galow, A.M., Rebl, A., Koczan, D., Bonk, S.M., Baumann, W., Gimsa, J., 2017. Increased osteoblast viability at alkaline pH in vitro provides a new perspective on bone regeneration. Biochem. Biophys. Rep. 10.
Gong, C., Fang, S., Xia, K., Chen, J., Guo, L., Guo, W., 2021. Enhancing the mechanical properties and cytocompatibility of magnesium potassium phosphate cement by incorporating oxygen-carboxymethyl chitosan. Regen. Biomater. 8 (1), rbaa048.
Grubbs, R., 1991. Effect of epidermal growth factor on magnesium homeostasis in BC3H1 myocytes. Am. J. Physiol. 260, C1158–1164.
Guan, J., Gao, C., Feng, L., Shen, J., 2001. Surface modification of polyurethane for promotion of cell adhesion and growth 1: surface photo-grafting with N,N-dimethylaminoethyl methacrylate and cytocompatibility of the modified surface. J. Mater. Sci. Mater. Med. 12 (5), 447–452.
Hassanajili, S., Karami-Pour, A., Oryan, A., Talaei-Khozani, T., 2019. Preparation and characterization of PLA/PCL/HA composite scaffolds using indirect 3D printing for bone tissue engineering. Mater. Sci. Eng. C Mater. Biol. Appl. 104, 109960.
He, L., Liu, X., Rudd, C., 2021. Additive-Manufactured gyroid scaffolds of magnesium oxide, phosphate glass fiber and polylactic acid composite for bone tissue engineering. Polymers 13 (2), 270.
Hickey, D., Ercan, B., Sun, L., Webster, T., 2015. Adding MgO nanoparticles to hydroxyapatite-PLLA nanocomposites for improved bone tissue engineering applications. Acta Biomater. 14, 175–184.
Holmes, B., Bulusu, K., Plesniak, M., Zhang, L., 2016. A synergistic approach to the design, fabrication and evaluation of 3D printed micro and nano featured scaffolds for vascularized bone tissue repair. Nanotechnology 27 (6), 64001.
Houaoui, A., Lyyra, I., Agniel, R., Pauthe, E., Massera, J., Boissière, M., 2020. Dissolution, bioactivity and osteogenic properties of composites based on polymer and silicate or borosilicate bioactive glass. Mater. Sci. Eng. C Mater. Biol. Appl. 107, 110340.
James, M., Anderson, Matthew, S., Shive, 2012. Biodegradation and biocompatibility of PLA and PLGA microsphere. Adv. Drug Deliv. Rev. 64 (1), 72–82.
Li, X., Xu, P., Cheng, Y., Zhang, W., Zheng, B., Wang, Q., 2020. Nano-pearl powder/chitosan-hyaluronic acid porous composite scaffold and preliminary study of its osteogenesis mechanism. Mater. Sci. Eng. C Mater. Biol. Appl. 111, 110749.
Lin, Z., Wu, J., Qiao, W., Zhao, Y., Wong, K., Chu, P., Yeung, K., 2018. Precisely controlled delivery of magnesium ions thru sponge-like monodisperse PLGA/nano-MgO-alginate core-shell microsphere device to enable in-situ bone regeneration. Biomaterials 174, 1–16.
Liu, K., Li, W., Chen, S., Wen, W., Luo, B., 2020. The design, fabrication and evaluation of 3D printed gHNTs/gMgO whiskers/PLLA composite scaffold with honeycomb microstructure for bone tissue engineering. Compos. B Eng. 192, 108001.
Lu, X., Xiong, S., Chen, Y., Zhao, F., Hu, Y., Guo, Y., Yang, B., 2020. Effects of statherin on the biological properties of titanium metals subjected to different surface modification. Colloids Surf., B 188, 110783.
Masuko, T., 1998. Crystallization behaviour of poly(l-lactide). Polymer.
Meng, D., James, R., Laurencin, C.T., Kumbar, S.G., 2012. Nanostructured polymeric scaffolds for orthopaedic regenerative engineering. IEEE Trans. NanoBioscience 11 (1), 3–14.
Mohd Zaffarin, A., Ng, S., Ng, M., Hassan, H., Alias, E., 2021. Nano-hydroxyapatite as a delivery system for promoting bone regeneration in vivo: a systematic review. Nanomaterials 11 (10).
Naghieh, S., Foroozmehr, E., Badrossamay, M., Kharaziha, M., 2017. Combinational processing of 3D printing and electrospinning of hierarchical poly(lactic acid)/gelatin-forsterite scaffolds as a biocomposite: mechanical and biological assessment. Mater. Des. 128–135.
Nonoyama, T., Wang, L., Tsuda, M., Suzuki, Y., Kiyama, R., Yasuda, K., Gong, J., 2021. Isotope microscopic observation of osteogenesis process forming robust bonding of double network hydrogel to bone. Adv. Healthc. Mater. 10 (3), e2001731.
On, S.W., Cho, S.W., Byun, S.H., Yang, B.E., 2020. Bioabsorbable osteofixation materials for maxillofacial bone surgery: a review on polymers and magnesium-based materials. Biomedicines 8 (9), 300.
Park, J., Kim, Y., Jang, J., Song, H., 2010. Osteoblast response to magnesium ion-incorporated nanoporous titanium oxide surfaces. Clin. Oral Implants Res. 21 (11), 1278–1287.
Pei, A., Qi, Z., Berglund, L.A., 2010. Functionalized cellulose nanocrystals as biobased nucleation agents in poly(l-lactide) (PLLA) – crystallization and mechanical property effects. Compos. Sci. Technol. 70 (5), 815–821.
Raisz, L.G., 1969. Effect of phosphate, calcium and magnesium on bone resorption and hormonal responses in tissue culture. Endocrinology (3), 446–452.
Russias, J., Saiz, E., Nalla, R.K., Gryn, K., Ritchie, R.O., Tomsia, A.R., 2006. Fabrication and mechanical properties of PLA/HA composites: a study of in vitro degradation. Mater. Sci. Eng. C Biomimet. Supramol. Syst. 26 (8), 1289–1295.
Salamanca, E., Pan, Y., Sun, Y., Hsueh, H., Dorj, O., Yao, W., Chang, W., 2022. Magnesium modified β-tricalcium phosphate induces cell osteogenic differentiation in vitro and bone regeneration in vivo. Int. J. Mol. Sci. 23 (3).
Serre, C., Papillard, M., Chavassieux, P., Voegel, J., Boivin, G., 1998. Influence of magnesium substitution on a collagen-apatite biomaterial on the production of a calcifying matrix by human osteoblasts. J. Biomed. Mater. Res. 42 (4), 626–633.
Shuai, C., Li, Y., Feng, P., Guo, W., Yang, W., Peng, S., 2018. Positive feedback effects of Mg on the hydrolysis of poly- l -lactic acid (PLLA): promoted degradation of PLLA scaffolds. Polym. Test. 68, 27–33.
Shuai, C., Li, Y., Wang, G., Yang, W., Peng, S., Feng, P., 2019a. Surface Modification of Nanodiamond: toward the Dispersion of Reinforced Phase in Poly-L-Lactic Acid Scaffolds. Elsevier Science.
Shuai, C., Zan, J., Qi, F., Wang, G., Peng, S., 2019b. nMgO-incorporated PLLA bone scaffolds: enhanced crystallinity and neutralized acidic products. Mater. Des. 174, 107801.
Swain, S., Bhaskar, R., Gupta, M.K., Sharma, S., Kumar, P., 2021. Mechanical, electrical, and biological properties of mechanochemically processed hydroxyapatite ceramics. Nanomaterials 11 (9), 2216(2211-2214).
Tan, J., Wang, D., Cao, H., Qiao, Y., Zhu, H., Liu, X., 2018. Effect of local alkaline microenvironment on the behaviors of bacteria and osteogenic cells. ACS Appl. Mater. Interfaces 10 (49), 42018–42029.
Tarafder, S., Davies, N.M., Bandyopadhyay, A., Bose, S., 2013. 3D printed tricalcium phosphate bone tissue engineering scaffolds: effect of SrO and MgO doping on in vivo osteogenesis in a rat distal femoral defect model. Biomaterialsence 1.
Tyler, B., Gullotti, D., Mangraviti, A., Utsuki, T., Brem, H., 2016. Polylactic acid (PLA) controlled delivery carriers for biomedical applications. Adv. Drug Deliv. Rev. 107, 163–175.
Wagener, V., Schilling, A., Mainka, A., Hennig, D., Gerum, R., Kelch, M., Virtanen, S., 2016. Cell adhesion on surface-functionalized magnesium. ACS Appl. Mater. Interfaces 8 (19), 11998–12006.
Wang, X., Song, G., Tao, L., 2010. Fabrication and characterization of nano-composite scaffold of PLLA/silane modified hydroxyapatite. Med. Eng. Phys. 32 (4), 391–397.
Xia, S., Liu, X., Wang, J., Kan, Z., Chen, H., Fu, W., Li, Z., 2019. Role of poly(ethylene glycol) grafted silica nanoparticle shape in toughened PLA-matrix nanocomposites. Composites 168 (JUL.1), 398–405.
Yuan, W., Li, B., Chen, D., Zhu, D., Zheng, Y., 2018. Formation mechanism, corrosion behavior, and cytocompatibility of microarc oxidation coating on absorbable high-purity zinc. ACS Biomater. Sci. Eng. 5 (2).
Yun, Z., Bei, L., Chen, Y., Chen, M., 2016. Effects of MgO whiskers on mechanical properties and crystallization behavior of PLLA/MgO composites. Mater. Des. 89 (JAN), 573–581.
Zahedi, S.A., 2019. 3D printing of bone scaffolds with hybrid biomaterials. Compos. B Eng.
Zhao, C., Wu, H., Ni, J., Zhang, S., Zhang, X., 2017. Development of PLA/Mg composite for orthopedic implant: tunable degradation and enhanced mineralization. Compos. Sci. Technol. 147 (jul.28), 8–15.
Zhao, Y., Liu, B., Bi, H., Yang, J., Li, W., Liang, H., Chen, M., 2018. The degradation properties of MgO whiskers/PLLA composite in vitro. Int. J. Mol. Sci. 19 (9).
Zhou, K., Yu, P., Shi, X., Ling, T., Zeng, W., Chen, A., Zhou, Z., 2019. Hierarchically porous hydroxyapatite hybrid scaffold incorporated with reduced graphene oxide for rapid bone ingrowth and repair. ACS Nano 13 (8), 9595–9606.
Zreiqat, H., Howlett, C., Zannettino, A., Evans, P., Schulze-Tanzil, G., Knabe, C., Shakibaei, M., 2002. Mechanisms of magnesium-stimulated adhesion of osteoblastic cells to commonly used orthopaedic implants. J. Biomed. Mater. Res. 62 (2), 175–184.